

Influence of Thermal Aging on Tensile and Low Cycle Fatigue Behavior of Type 316LN Austenitic Stainless Steel Weld Joint



T. SURESH KUMAR, A. NAGESHA, J. GANESH KUMAR, P. PARAMESWARAN,
and R. SANDHYA

Influence of short-term thermal aging on the low-cycle fatigue (LCF) behavior of 316LN austenitic stainless steel weld joint with 0.07 wt pct N has been investigated. Prior thermal exposure was found to improve the fatigue life compared with the as-welded condition. Besides, the treatment also imparted a softening effect on the weld metal, leading to an increase in the ductility of the weld joint which had a bearing on the cyclic stress response. The degree of cyclic hardening was seen to increase after aging. Automated ball-indentation (ABI) technique was employed toward understanding the mechanical properties of individual zones across the weld joint. It was observed that the base metal takes most of the applied cyclic strain during LCF deformation in the as-welded condition. In the aged condition, however, the weld also participates in the cyclic deformation. The beneficial effect of thermal aging on cyclic life is attributed to a reduction in the severity of the metallurgical notch leading to a restoration of ductility of the weld region. The transformation of δ -ferrite to σ -phase during the aging treatment was found to influence the location of crack initiation. Fatigue cracks were found to initiate in the base metal region of the joint in most of the testing conditions. However, embrittlement in the weld metal caused a shift in the point of crack initiation with increasing strain amplitude under LCF.

<https://doi.org/10.1007/s11661-018-4690-4>

© The Minerals, Metals & Materials Society and ASM International 2018

I. INTRODUCTION

LOW-CYCLE fatigue (LCF) is an important design consideration in components operating at elevated temperatures. Austenitic stainless steels are extensively used in the construction of various components of sodium-cooled fast reactors (SFRs). Type 316LN austenitic stainless steel (316LN SS) containing 0.02 to 0.03 wt pct carbon and 0.07 to 0.08 wt pct nitrogen is the preferred structural material for the primary side components such as the main vessel, the inner vessel, and the intermediate heat exchanger of SFRs in view of its microstructural stability, coupled with an excellent combination of mechanical and chemical properties, good weldability, and compatibility with the liquid sodium coolant.^[1] However, a low thermal conductivity

and a high thermal expansion coefficient of the alloy result in significant amounts of thermal stresses during startup and shutdown operations and thermal fluctuations in liquid metal coolant of the reactor. The repetition of the above processes induces strain-controlled LCF loading. Fabrication of large components inevitably involves numerous weld joints that are microstructurally and mechanically heterogeneous. It is well recognized that the integrity of a welded structure is largely dictated by the properties of the weld joint. Fatigue-life evaluation of the weldments, though, has traditionally been based on the properties of the base metal, factored by an appropriate safety margin to account for the material and the geometric discontinuities. This is mainly due to the inadequate database available on creep, fatigue, and creep-fatigue interaction properties of the welds and weldments. Better understanding of the behaviors of welds would add to the confidence in design and associated safety factors. In SFRs, many primary side components inside the reactor vessel are inaccessible for in-service inspection, and hence, the resistance to surface microcrack initiation/propagation is of utmost importance in the overall fatigue behavior of such components.

T. SURESH KUMAR is with the Homi Bhabha National Institute, Kalpakkam, Tamil Nadu, 603102, India. A. NAGESHA, J. GANESH KUMAR, and R. SANDHYA are with the Materials Development and Technology Division, Indira Gandhi Centre for Atomic Research, Kalpakkam, Tamil Nadu, 603102, India. Contact e-mail: nagesh@igcar.gov.in P. PARAMESWARAN is with the Physical Metallurgy Division, Indira Gandhi Centre for Atomic Research, Kalpakkam, Tamil Nadu, 603102, India.

Manuscript submitted September 12, 2017.

Article published online May 23, 2018

A significant problem encountered with the production of fully austenitic stainless steel welds is their tendency to hot cracking and microfissuring. In order to minimize these damages, the composition of the welding consumables is adjusted in such a way that a primary ferritic mode of solidification results, with a small amount of δ -ferrite retained in the weld deposit.^[2] The δ -ferrite is only stable at high temperature while existing as a metastable phase in the austenitic matrix at room temperature. Upon exposure to elevated temperatures, the above phase transforms into various types of phases such as secondary austenite, sigma, chi, laves, and carbides depending on the chemical composition, and the temperature and time of exposure.^[3-6] The embrittlement arising out of hard and brittle σ -phase precipitation in the weld metal microstructure is generally reported to have adverse consequences on the mechanical properties.^[7-10] For design and safety assessment of structures and their components for high-temperature use, a thorough knowledge of the fatigue crack initiation and growth is of paramount importance. The data pertaining to LCF available on Type 316 SS weld joints^[11-16] are related to the as-welded condition without considering the influence of in-service thermal exposure. Since the structural components of SFRs are likely to be exposed to temperatures in the range from 623 K to 873 K (350 °C to 600 °C) for extended durations, a thorough knowledge of the metallurgical transformations and the evolution of mechanical properties thereof, assumes importance. At high temperatures, the deformation and fracture behaviors of the weldments are significantly influenced by the kinetics of the δ -ferrite transformation. A general reduction in the creep properties due to transformation of δ -ferrite in austenitic stainless steel welds upon exposure to elevated

temperatures has been reported in literature.^[17] Goyal *et al.*^[18] reported that thermal aging at 873 K (600 °C) / 10,000 hours results in a complete transformation of the δ -ferrite, leading to an increase in the stress response and a reduction in the LCF life compared with the as-welded condition. It is important to have a clear insight on how the different regions of the weld joint respond to external loading, for gaining a comprehensive understanding of the complex behavior of the weldment. The strain distribution in a welded joint in response to an externally applied load is greatly influenced by the relative stiffness of individual zones in the weld joint, such as the base metal, the heat-affected zone (HAZ), and the weld metal. An understanding of the overall response of the weldment to external loading therefore requires a thorough knowledge of the behavior of the different zones. In this context, automated ball-indentation (ABI) technique has found widespread application for investigating local variation of mechanical properties at different temperatures in several alloys including base metals^[19-22] and weldments.^[23-28] The present study was initiated to gain a comprehensive understanding on the influence of short-term (973 K (700 °C)/2 hours) thermal exposure on the LCF behavior of 316LN SS weld joint as a function of the strain amplitude and temperature.

II. EXPERIMENTAL

A. Welding and Thermal Aging

316 LN SS base metal in the form of 25 mm thick mill-annealed plates were used for preparing the weld pads. The plates were cut into 250 × 245 mm pieces and machined into a double-V configuration, with an included angle of 35 deg, as shown in Figure 1. They were then joined perpendicular to the rolling direction (along the 245 mm side) using shielded metal arc welding process, employing a joint geometry as shown in Figure 1. Type E316-15 (modified) welding electrodes with 3.15 mm diameter were used after soaking for 1 hour at 473 K (200 °C) prior to welding. Optical emission spectrometry (OES) was used for the elemental analysis of the base metal and the weld metal. In OES, the spark generated between an electrode and the metal sample brings the vaporized atoms to a high-energy state within the discharge plasma. These excited atoms and ions create a unique emission spectrum specific to the presence and concentration of the individual elements. The intensity of the spectrum processed by the detectors in argon atmosphere gives the qualitative and quantitative analysis of the elements. Chemical compositions of the base metal and

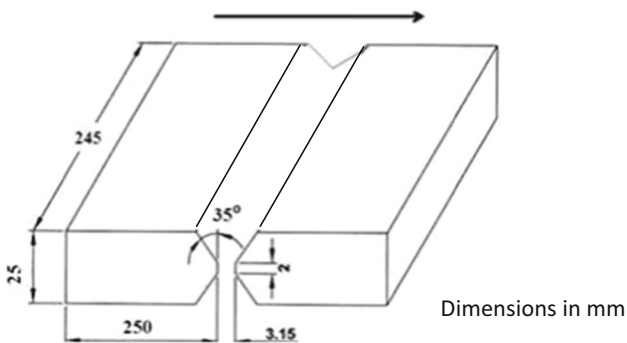


Fig. 1—Weld pad configuration used for preparing the weld joints (arrow indicates the rolling direction).

Table I. Chemical Composition of the E316-15 (Modified) Electrode and 316L (N) Base Metal in Weight Percent

Material	C	Mn	Ni	Cr	Mo	N	S	P	Fe
Base metal	0.03	1.7	12.2	17.5	2.5	0.07	0.0055	0.013	bal
Filler metal	0.05	1.4	11.1	18.9	2.0	0.12	0.009	0.02	bal

filler metal (electrode) are presented in Table I. The voltage and current were maintained at approximately 25 V and 150 A, respectively, during welding, which was carried out with an interpass temperature of 423 K (150 °C). The weld pads were subjected to X-Radiography for their soundness, and samples were machined from defect-free regions of the pads. With a view to investigate the thermal aging effects on the LCF behavior, a few blanks were exposed to 973 K (700 °C) for 2 hours. The samples were etched in modified Murakami's reagent (30 g KOH, 30 g K₃[Fe(CN)₆], and 150 ml water) at 363 K (90 °C) for 20 to 30 seconds for examining the microstructure of the weld zone. The δ -ferrite contents of the as-welded and aged specimens were determined using a Fischer Feritscope[®], which generates a magnetic field on the sample surface through an induction coil that interacts with the magnetic components of the specimen. The change in the magnetic field induces a voltage in proportion to the magnetic (δ -ferrite in the present case) content in the sample.

B. Tensile and Hardness Testing

Tensile tests were conducted at 873 K (600 °C) using a nominal strain rate of $3 \times 10^{-4} \text{ s}^{-1}$ in both the as-welded and thermally aged conditions. Microhardness measurements were made using a Vickers hardness tester, employing a load of 200 g with a dwell period of 15 seconds. ABI tests were performed on the non-LCF and LCF-cycled (temperature: 873 K (600 °C), strain amplitude ($\Delta\epsilon_t/2$): ± 0.4 pct, cycled to saturation, *i.e.*, ≈ 150 cycles) joints in both the as-welded and aged conditions at a temperature of 873 K (600 °C) toward understanding the response of individual zones to the cyclic loading.

C. Low Cycle Fatigue Testing

Fully reversed strain-controlled isothermal LCF tests were conducted in air using a ± 100 kN servohydraulic fatigue testing machine equipped with an induction heating facility. The tests were carried out at temperatures of 823 K, 873 K, and 923 K (550 °C, 600 °C, and 650 °C) employing $\Delta\epsilon_t/2$ of ± 0.25 , ± 0.4 and ± 0.6 pct at a constant strain rate of $3 \times 10^{-3} \text{ s}^{-1}$ in the as-welded and aged (973 K (700 °C)/2 hours) conditions, using tubular samples as shown in Figure 2. Besides, one LCF test was performed at 923 K (650 °C) with a $\Delta\epsilon_t/2$ of ± 0.4 pct at a strain rate of $3 \times 10^{-3} \text{ s}^{-1}$ on the base metal sample, for the sake of comparison with the weld joint behavior. The cyclic life was defined as the number of cycles corresponding to a 20 pct drop in tensile stress from the saturated / half-life value. The failed samples were longitudinally cut from close to the fracture region and examined with optical microscope after electrolytic etching in a solution containing 60 pct HNO₃ in water using a voltage of 1.5 V. Fatigue crack initiation and propagation modes were characterized through optical microscopy and scanning electron microscopy (SEM) and dislocation substructure was studied by transmission electron microscopy (TEM). Specimens for the TEM examination were taken from regions close to the fracture surface and thinned down manually to a thickness of 0.1 mm prior to electrolytic thinning in a solution containing 20 pct perchloric acid and 80 pct methanol at 235 K (− 38 °C), using a voltage of 10 to 15 V.

III. RESULTS AND DISCUSSION

A. Microstructure in As-welded and Thermally Aged Conditions

The weld metal presented a complex microstructure of austenite with δ -ferrite (Figure 3). The microstructure

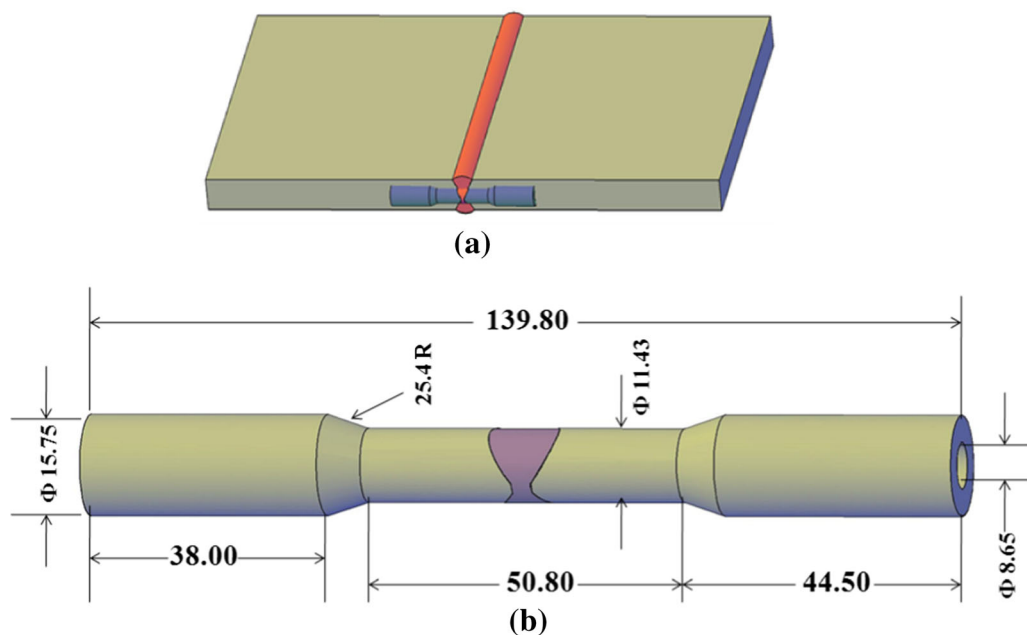


Fig. 2—(a) Orientation of the specimen with respect to the weld pad and (b) geometry of test specimen (all dimensions are in mm).

across the weld metal was highly heterogeneous with different morphologies of δ -ferrite. The region close to the weld root presented a globular morphology on account of the repeated thermal cycles imposed during successive passes. However, the test section largely composed of a vermicular morphology, as presented in Figure 3.

The aging treatment of 973 K (700 °C)/2 hours was aimed at capturing the long-term effects at the lower reactor-operating temperatures of 823 K to 873 K (550 °C to 600 °C). In the weld metal, carbides, intermetallic σ , and some untransformed δ -ferrite have been identified in the aged condition as shown in Figure 4. The δ -ferrite acts as a nucleation site for all the transformations in the weld zone upon exposure to high temperatures. Among all the phases reported in 316 SS weld metal, the σ -phase is reported to be thermodynamically the most stable phase.^[3,6]

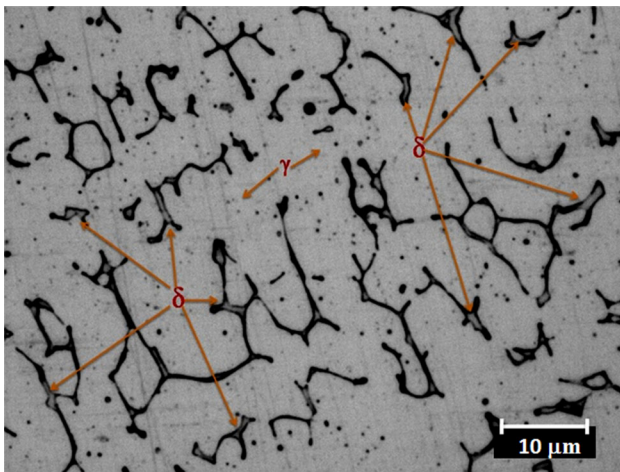


Fig. 3—Optical micrograph of vermicular δ -ferrite in weld metal in the as-welded condition.

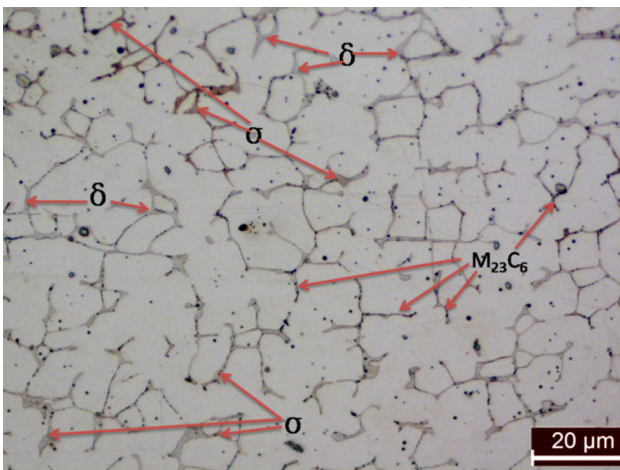


Fig. 4—Optical micrograph of the sample aged at 973 K (700 °C) for 2 h, showing the presence of secondary phases like $M_{23}C_6$ and sigma phase with δ -ferrite.

Thermal aging resulted in a breakdown of the continuous network of austenite/ferrite interface. In the present material, the amount of carbide precipitation is low owing to the low carbon content, leaving the δ -ferrite with a higher amount of Cr and Mo. This renders the precipitation of σ -phase easier, as it only requires a crystallographic change for the transformation to occur. The morphology of σ -phase after the aging treatment is similar to that of the initial δ -ferrite, indicating that the transformation initiated in the δ -ferrite.

B. Delta Ferrite and Microhardness

The ferrite number (FN) was found to vary along the length and width of the weld and from bead to bead. The average δ -ferrite content within the test section of the weld zone was found to be 7.2 FN in the as-welded condition. However a reduction in the same to about 2.8 FN was noted following the aging treatment owing to the transformation of δ -ferrite to σ -phase and carbides. Variations in grain size and δ -ferrite content across all the regions of the weld joint in both the as-welded and the aged conditions are presented in Table II. The variation in microhardness values across the weld joint in the as-welded and aged conditions is presented in Figure 5.

The weld metal in the as-welded condition exhibited a higher hardness than the base metal due to its inhomogeneous cast structure and higher amounts of Cr, C, and N as shown in Table I. A reduction in hardness was observed in the weld metal region upon thermal aging (Figure 5) as a result of decrease in the dislocation density and transformation of δ -ferrite.

C. Tensile Properties of the Weld Joint

The yield strength (YS) in the aged condition was seen to be 191 MPa, which is slightly lower than 200 MPa shown by the as-welded joint. The above result is in agreement with the findings of Thomas and Yapp^[3] and Gill *et al.*^[29] who reported a reduction in the YS upon aging at 973 K (700 °C). Thomas and Yapp^[3] attributed the reduction in the YS to thermal recovery, whereas Gill *et al.*^[29] reported that the decrease in YS is a consequence of the dissolution of δ -ferrite, depletion of the austenite matrix of solid solution strengtheners such as C, N, Cr, and Mo due to formation of carbides and other intermetallics. In addition, softening of the weld

Table II. Variations in Grain Size and δ -Ferrite Content Across All the Regions of the Weld Joint

Condition	Region	Grain Size (μm)	δ -Ferrite (FN)
As-welded	base metal	102-107	—
	HAZ	135-142	0.7
	weld metal	—	7.2
Aged [973 K (700 °C)/2 h]	base metal	102-106	—
	HAZ	135-142	—
	weld metal	—	2.8

metal region takes place due to annihilation of dislocations of opposite sign. Although the aged material shows a lower YS, the ultimate tensile strength (UTS) is identical in both the conditions (Table III), which is indicative of a higher work hardening in the aged condition. Besides, a significant increase in the ductility of the weld joint after thermal aging was observed, as can be seen from Table III. This could be ascribed to the recovery effects associated with the relief of thermal stresses and the softening effects taking place in the weld metal region during the prior thermal exposure. In the as-welded condition under tensile loading, the base metal part of the weld joint bears the major part of the applied strain and undergoes extensive deformation, with the response of the weld region to the applied load being negligible. This can be clearly seen in the image presented in Figure 6 which shows the concentration of deformation in the base metal portion that finally led to a cup-and-cone type of failure.

D. Characterization Through ABI

The indentation profile during an ABI test is shown schematically in Figure 7.^[22]

The symbols h_e , h_p , and h_t in the Figure 7 denote, respectively, the elastic, plastic, and total indentation depths; and d_p and d_t are the plastic and total indentation diameters obtained during loading and partial unloading sequences, respectively, of the ABI testing. D is the diameter of the indenter. The applied indentation

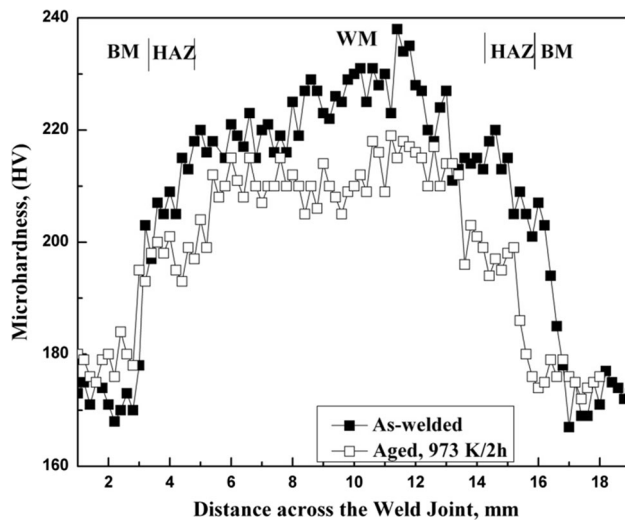


Fig. 5—Variation of microhardness across the weld joint.

loads and associated penetration depths are used to calculate the tensile properties and incremental stress–strain values from a combination of elasticity and plasticity theories and semiempirical relationships governing material behavior under multiaxial indentation loading. The load vs depth of indentation curves obtained from the ABI tests for the base and weld metal regions of the weld joint are presented in Figure 8.

The above figure shows the behaviors of the weld metal and base metal portions of the weld joint in the as-welded and aged conditions under both the non-LCF and LCF-cycled (up to saturation) conditions at 873 K (600 °C). Prior to LCF, the weld metal portion showed a higher load response compared with the base in the as-welded condition. Under the LCF cycle condition, however, the base metal displayed a higher load response compared with the welds in both the as-welded

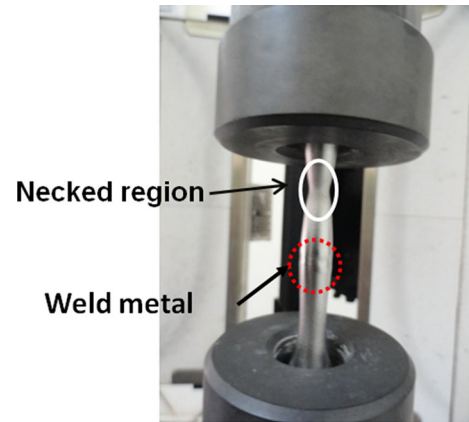


Fig. 6—Concentration of deformation in the base metal region during tensile testing of the weld joint in the as-welded condition.

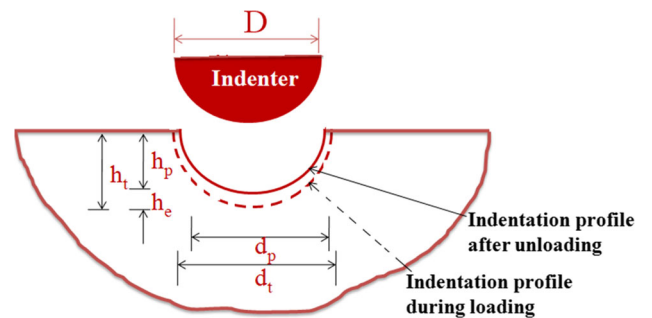


Fig. 7—Schematic of indentation profile during an ABI test, adapted from Ref. [22].

Table III. Tensile and Hardness Properties at 873 K in Both the As-welded and Aged Conditions

Property	As-welded	Aged [973 K (700 °C)/2 h]
Yield strength (MPa)	200	191
Ultimate tensile strength (MPa)	407	405
Elongation (pct)	23	27
Reduction in area (pct)	52	58
Microhardness (average, HV _{0.2})	230	215

and aged conditions. The load vs depth of indentation data obtained from the base and the weld metal portions were analyzed according to the procedure outlined in Annexure- I to determine the local tensile properties.

E. Variation of Tensile Properties

1. Yield and ultimate tensile strength

The base metal and weld metal regions showed clear variations in the tensile properties in the non-LCF and LCF-cycled conditions. The weld region showed higher YS compared with the base under all conditions, as seen from Figure 9. Thermal aging resulted in a significant decrease in the YS of the weld metal compared with the as-welded condition. This is consistent with the variation of microhardness observed between the as-welded and aged conditions, described earlier. The δ -ferrite transformation and recovery effects as described earlier are the main mechanisms responsible for the decrease in the YS subsequent to aging.

Upon cycling to saturation of the as-welded joint, a significant increase in the YS was observed in the base metal portion of the joint in comparison with the specimen which was not exposed to LCF cycling. This was accompanied by a slight decrease of the same in the weld metal part, as seen from the Figure 9. The increase in YS of the base metal region after LCF loading to saturation could be attributed to its homogeneous austenitic structure, which experienced considerable work hardening during cyclic deformation. In contrast to the above, the decrease in YS of the weld metal region is due to the cyclic softening that follows consequent to the significant reduction in the dislocation density and recovery effects.^[11] However, LCF cycling to the saturation of the thermally aged joint led to increases in the YS values of both the base as well as the weld metal regions, with the extent of increase in the weld zone being marginally higher compared with the base metal (Figure 9). This is indicative of the plastic deformation

taking place in the weld metal zone which has been softened by the prior thermal aging. It can be inferred from the above observation that the base metal takes most of the applied cyclic strain during LCF deformation in the as-welded condition and undergoes significant hardening. However, after the thermal exposure, a higher response of the weld metal to the applied cyclic strain was observed resulting in a significant strain hardening compared with the as-welded condition.

The UTS values exhibited by the base metal and weld metal were also found to be different in the as-welded and aged conditions, as presented in Figure 10. In the non-LCF condition, the weld metal showed higher UTS in the aged condition compared with the as-welded condition. However, the weld region both the as-welded and aged conditions showed a decrease in the UTS after cyclic saturation, with the extent of decrease being greater in the aged condition compared with the as-welded condition. This signifies embrittlement of

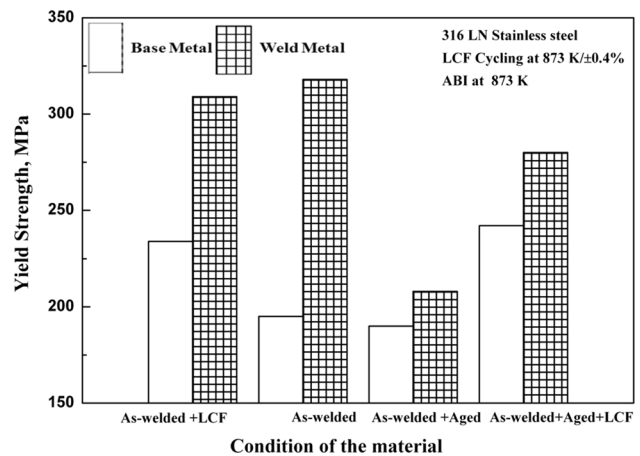


Fig. 9—Variation of yield strengths of the base and weld metal regions of the weld joint in the non-LCF and LCF-cycled conditions.

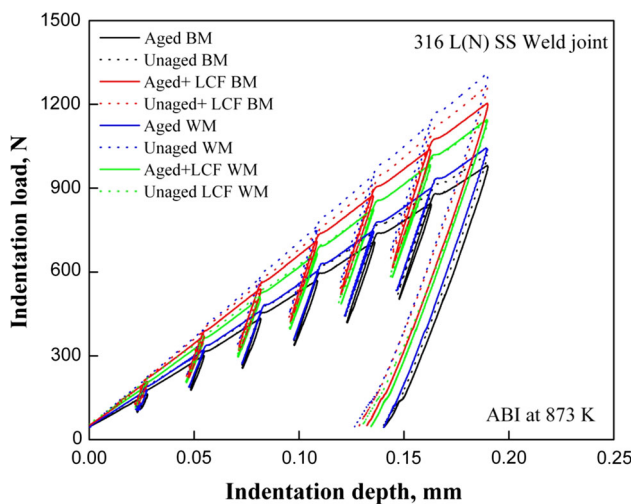


Fig. 8—Load vs depth of indentation data obtained through ABI on 316LN SS weld joint at 873 K (600 °C).

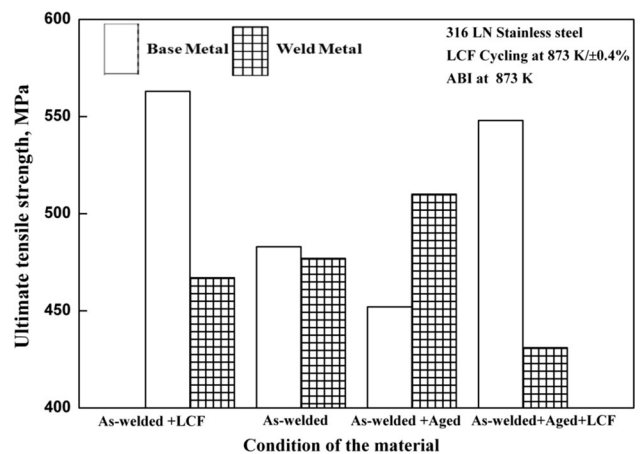


Fig. 10—Variations of ultimate tensile strength of the base and weld metal regions of the weld joint in non-LCF and LCF-cycled conditions.

the weld zone upon cyclic deformation which could be attributed to the formation of σ -phase and carbides. It may be noted that while the austenite is a soft phase and can accommodate higher strains, the σ -phase has limited ductility and strain accommodation capacity. Besides, cyclic deformation also accelerates the transformation of δ -ferrite into σ -phase and carbides, which may be attributed to the enhancement of diffusion rate due to the increased vacancy generation associated with cyclic deformation.^[9,11,15] The consequent embrittlement in the weld metal resulted in a lower strain hardening capacity of the weld metal after LCF cycling, which will be discussed later in Section III-E-3.

2. True stress–true strain response

The significant variation in the local material properties (YS, UTS) can cause a corresponding localization of strain in the constituents of the weld joint. Figure 11 presents the true stress–true strain plots obtained through ABI tests on the weld joint under different conditions. In the non-LCF condition, the higher strength of the weld metal part resulted in a higher stress–strain response compared with the base metal in both the as-welded and aged conditions. Following LCF cycling to the saturation, however, the stress–strain response of the base metal was found to be higher than that of the weld metal as a result of the strain hardening induced in the former, during the cyclic loading. This could be attributed to the fact that the base metal with its ductile austenite matrix takes higher amount of strain due to the difference in the YS values between the base and weld regions of the weld joint. It can also be observed from Figure 11 that the plastic strain in the weld metal is much lower compared with the base metal for a given value of stress. The higher resistance of the weld region to the local deformation compared with the base metal imparts a *metallurgical notch* effect in the joint. Prior thermal exposure causes a significant softening in the weld portion as a consequence of which, the deformation gets more uniformly spread out across the

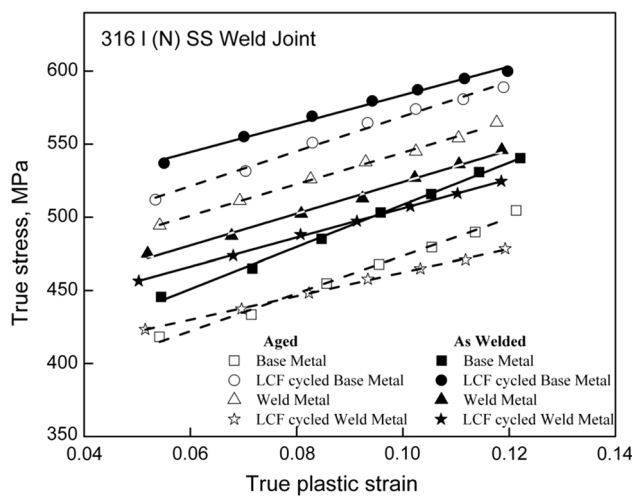


Fig. 11—Comparison of ABI-generated true stress–true plastic strain curves of weld metal and base metal regions of the weld joint at 873 K (600 °C).

joint. The severity of the metallurgical notch therefore gets reduced upon thermal aging. The weld metal in both the as-welded and aged conditions showed a lower stress–strain response in the LCF-cycled condition compared with the non-LCF cyclic condition as reflected in Figure 11.

3. Strain hardening exponent

Strain hardening exponents (n) were found to be 0.23 and 0.13, respectively, for the base metal and the weld metal regions in all cases, except under the thermally aged condition as shown in Figure 12.

Upon thermal aging, n showed a value of 0.23 in the weld region, equaling that of the base metal. This is indicative of the recovery of the work hardening capacity of the weld zone, consequent to the aging treatment, which resulted in a decrease in the internal strain in the weld metal and rendered the material more work hardenable. Upon cycling of the aged joint to saturation under LCF, the value of n exhibited by the weld metal region reverted back from 0.23 to 0.13 as shown in the Figure 12. The above variations in n could be associated with the work hardening and the consequent embrittlement of the weld zone. It may be noted that the above results are in line with the variations in YS and microhardness upon thermal aging.

F. Comparison of Cyclic Stress Responses Between Base Metal and Weld Joint Under LCF

The cyclic stress response (CSR) of the base metal showed an initial pronounced cyclic hardening for the first 100 cycles, followed by a brief softening, leading to a saturation regime toward the end of life, as shown in Figure 13. The relative proportions of each of these regimes depend on the initial material condition as well as the microstructural changes that take place during the course of cycling. Formation and subsequent growth of macrocracks toward the end of test led to a marked reduction in the tensile stress. The observed CSR is characteristic of austenitic stainless steels containing

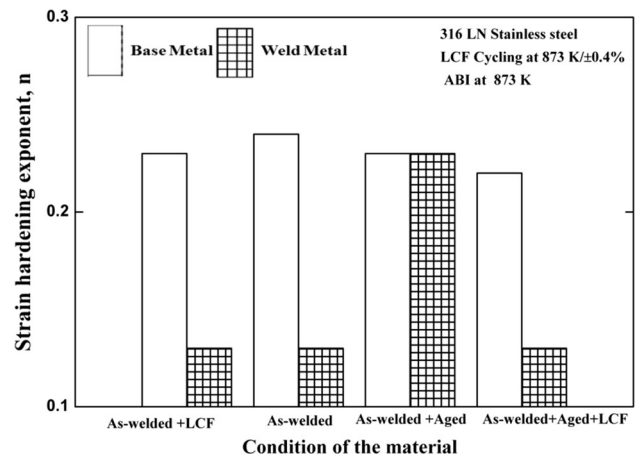


Fig. 12—Variation of the strain hardening exponents of the base and weld metal regions of the weld joint under the non-LCF- and LCF-cycled conditions.

interstitial strengthening elements and is in agreement with reports published by other authors on similar alloys.^[12,30–32]

The initial hardening in the base metal can be ascribed to (a) the increase in the dislocation density and mutual interaction among them, (b) the interaction between dislocations and solute atoms, and (c) the formation of fine precipitates on dislocations during cyclic loading.^[32] Sundararaman *et al.*^[33] emphasized on the formation of substitutional–interstitial complexes that lead to rapid initial strain hardening due to the increased resistance to dislocation motion in the matrix. Kim *et al.*^[34] attributed the initial cyclic hardening under LCF cycling in the temperature range from 573 K to 873 K (300 °C to 600 °C) in type 316LN SS, to dynamic strain aging (DSA). In contrast to the base metal, the weld joint exhibited a much shorter period of cyclic hardening in the first few cycles followed by a continuous and gradual softening regime during the major part of cycling at all strain amplitudes in the investigated temperature range from 823 K to 923 K (550 °C to 650 °C). The initial hardening of the weld joints is similar to that displayed by the base metal although the degree of hardening was significantly lower (Figure 13). This is to be expected, considering that the major part of the gauge length of the joint comprises of the base metal. However, at low-strain amplitudes, a near-saturation regime was observed as against a continuous softening seen at the higher strain amplitudes at all the temperatures as shown in Figures 14 and 15(a). Cyclic stress response of the weld joint represents a contribution from all the three regions, *viz.*, the base metal, the HAZ, and the weld metal. The weld joint displayed a relatively higher stress response compared with the base metal due to the presence of a microstructurally altered HAZ region together with a relatively harder weld zone with a high dislocation density. However, the differences in the CSR between the weld joint and the base metal decreased with progressive cycling, as shown in Figure 13.

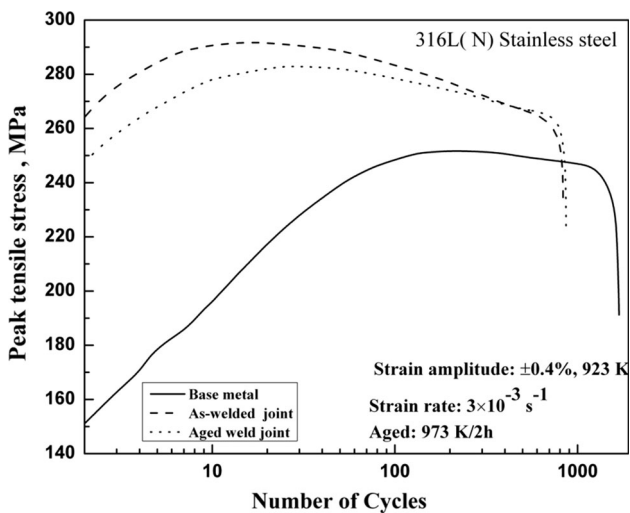


Fig. 13—Comparison of cyclic stress responses between base metal and weld joints at 923 K (650 °C).

G. Influence of Aging

1. Cyclic stress response

A distinct difference was observed between the CSR in the as-welded and aged conditions; the stress amplitude corresponding to the first cycle was found to be significantly lower in the aged condition compared with the as-welded condition (Figures 13 and 14). However, the difference in stress response was seen to diminish with the increasing number of LCF cycles as shown in Figure 15(b). This is due to the cyclic hardening induced in the weld metal region that had been rendered soft during the prior thermal aging. Furthermore, the initial hardening was observed to spread over a larger number of cycles in the aged condition in comparison with the as-welded condition, as shown in Figures 14 and 15. The extent of cyclic softening was observed to be higher in the as-welded condition compared with the aged condition, as presented in the above figures. The variation of half-life tensile stress with temperature for the two conditions at different strain amplitudes is presented in Figure 16.

The difference in stress response behaviors between the as-welded and aged conditions could be related to

- A higher dislocation density and a metastable δ -ferrite (with higher amounts of the strengthening solute elements, coupled with its high-energy state) of the weld metal, and
- Metallurgical transformations (δ -ferrite decomposition and carbide/nitride formation) and recovery effects.

The lower initial stress response shown by the aged weld joint could be ascribed to the softening effects as a result of a decrease in the dislocation density in the weld zone. Besides, the transformation of δ -ferrite to σ -phase also imparts a softening effect by causing a depletion of the strengthening elements, *i.e.*, Cr, Mo, C, and N from the matrix.

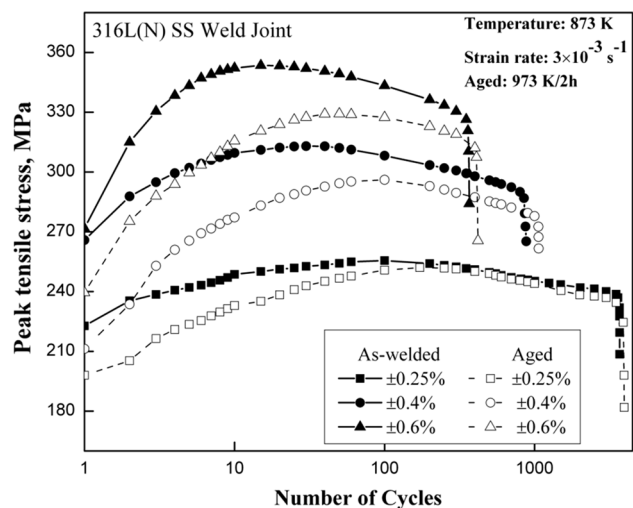


Fig. 14—Comparison of cyclic stress responses in the as-welded and aged conditions at 873 K (600 °C).

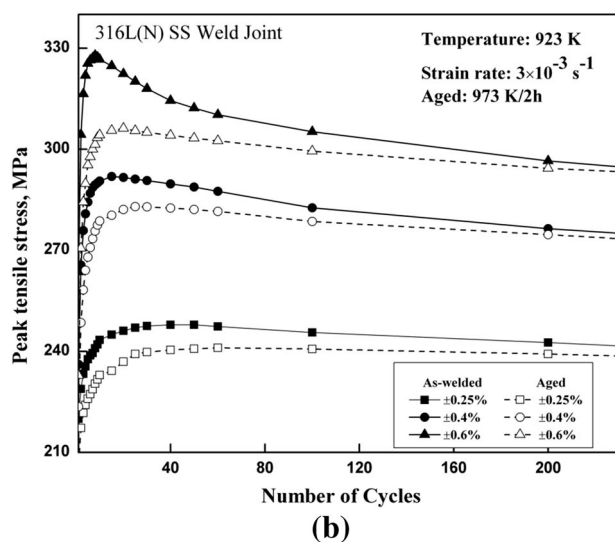
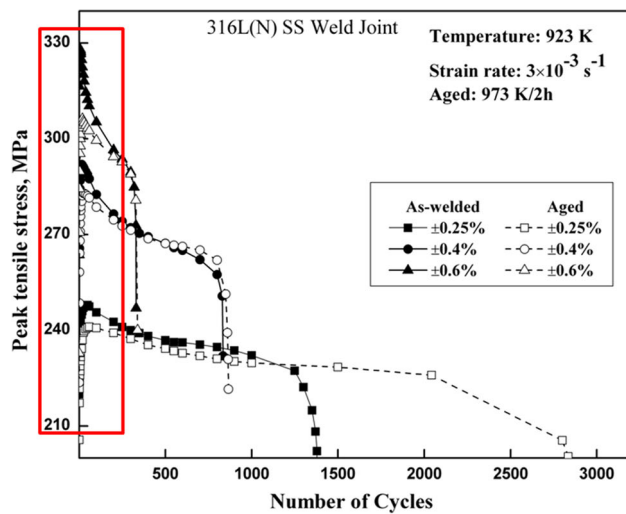


Fig. 15—(a) Comparison of cyclic stress responses in the as-welded and aged conditions at 923 K (650 °C). (b) Magnified view of the marked portion of Fig. 15(a) showing the initial period of cycling.

In the as-welded condition, considering the negligible precipitate concentration in the matrix and short duration of the LCF tests, contribution from precipitation to the initial cyclic hardening can be ruled out. The possible mechanisms for the initial hardening, therefore, are dislocation–dislocation and dislocation–solute atom interactions. In austenitic stainless steels, the solutes responsible for initial hardening have been identified to be carbon atoms at temperatures less than 573 K (300 °C) and Cr atoms in the temperature range from 673 K to 873 K (400 °C to 600 °C).^[35] Thermal aging studies on the 316 SS welds^[8,29] reported that heat treatment at 973 K (700 °C) for 2 hours is sufficient to cause precipitation of carbides/nitrides and other intermetallics like sigma and chi phases, depending on the composition. In the aged condition, besides σ -phase and δ -ferrite, the weld zone composed of very fine precipitates (Figure 4) which could also play a role in causing

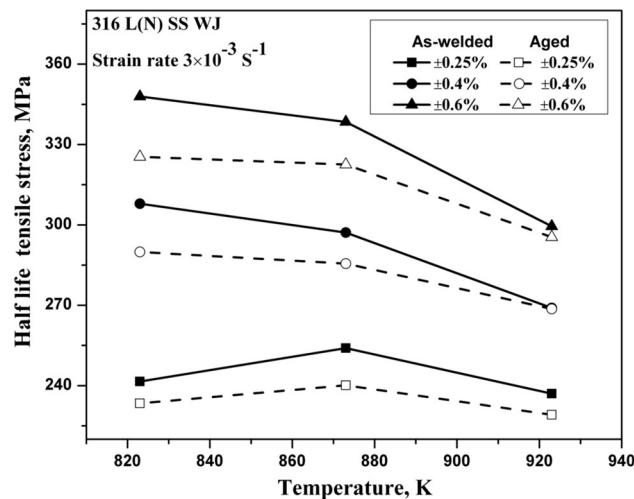


Fig. 16—Variation of half-life tensile stress under LCF as a function of temperature at different strain amplitudes in the as-welded and aged conditions.

the initial cyclic hardening. The initial cyclic hardening in aged condition may therefore be attributed to dislocation–dislocation and dislocation–precipitate interactions.

The occurrence of saturation at the lower strain amplitudes in the weld joint (Figure 14 and 15) is similar to the behavior exhibited by the base metal, indicating the predominance of deformation in the base metal part of the weld joint. Besides, the lower rate of cyclic softening observed at the lower strain amplitude also contributed to the near-saturation regime observed in the CSR. Cyclic softening occurs when the rate of annihilation of dislocations is greater than their generation rate, causing a net decrease in the dislocation density, or as a result of a rearrangement in the dislocation structure into low energy configuration.^[11] Gradual cyclic softening has been reported^[11] to have a correlation with the evolution of dislocation substructure from random to a well-defined cell structure, resulting in the lowering of stress response during cyclic deformation.

2. Degree of hardening and plastic strain amplitude

The aging-induced recovery and softening effects in the weld zone lead to a greater amount of cyclic hardening during successive cycling in the weld region. This resulted in an enhancement in the degree of hardening (defined as the ratio of the difference between the peak and the first cycle stress to the first cycle stress) in the weldment in the aged condition compared with the as-welded condition as presented in Figures 17(a) and (b). The extent of hardening was seen to be in direct proportion to the applied strain amplitude, as seen from Figure 17(a). With an increase in temperature, a reduction in the degree of hardening was observed as shown in Figure 17(b).

The plastic strain developed in the aged specimens in the beginning of the cycling was found to be higher than that of the as-welded specimens which is consistent with the lower YS shown by the former. However with the

progress of cycling, the difference in plastic strain amplitudes ($\Delta\epsilon_p/2$) between the as-welded and aged specimens was found to decrease. The above difference in the evolution of plastic strains for the two conditions is due to the initial softening and subsequent work hardening occurring in the weld metal.

The variation in the half-life $\Delta\epsilon_p/2$ with temperature in the as-welded and aged conditions is shown in Figure 18. The aged joint consistently showed a higher $\Delta\epsilon_p/2$ at half-life. With an increase in test temperature, $\Delta\epsilon_p/2$ was seen to increase, with the rate of increase being higher in the as-welded condition compared with the aged condition. The above difference is due to the softening effect induced under cyclic loading with increase in temperature. The higher softening rate in the as-welded condition resulted in an increased amount of cyclic plastic strain accumulation.

3. Influence of LCF cycling on the decomposition of δ -ferrite

The initial δ -ferrite contents in the gauge length of the specimen in the as-welded and aged conditions were 7.2 and 2.8 FN, respectively. Table IV presents the FN after LCF cycling at different temperatures and strain amplitudes in both the conditions, along with the percentage of transformation (with respect to the initial δ -ferrite content). The rate of decomposition of the δ -ferrite was higher in the as-welded condition, particularly at the strain amplitudes of ± 0.25 and ± 0.4 pct. This is only to be expected because the driving force for the transformation of δ -ferrite remains comparatively low owing to prior transformation that took place during the initial aging treatment. However, at the strain amplitude of ± 0.6 pct, the transformation in the aged condition was found to get accelerated, resulting in the pct transformation of δ -ferrite exceeding that observed in the as-welded condition, as shown in Figure 19.

As the precipitation of carbides and intermetallics are diffusion controlled, the continuous network of δ -ferrite and austenite is expected to provide an easy path for diffusion in the as-welded condition, which could lead to

a rapid transformation of the δ -ferrite. The above observation underscores a strong dependence of the decomposition rate of δ -ferrite on the strain amplitude of LCF, apart from the testing temperature (Table IV). Similar results were also reported by Hasebe and Asayama.^[36] The rate controlling step associated with the transformation δ -ferrite in 316(N) SS weld metal was reported to be the boundary diffusion of Cr atoms in the initial stages and lattice diffusion of Mo during the later stages when the δ -ferrite network has broken down.^[37]

4. Dislocation substructure

The dislocation substructure in the weld zone of the joint in the as-welded condition resembles that of a highly cold worked structure, characterized by a high dislocation density as shown in Figure 20. The high dislocation density could be attributed to the thermal stresses associated with the localized heating and cooling that occur during the overlapping of successive weld passes. Repeated exposure to heating and cooling

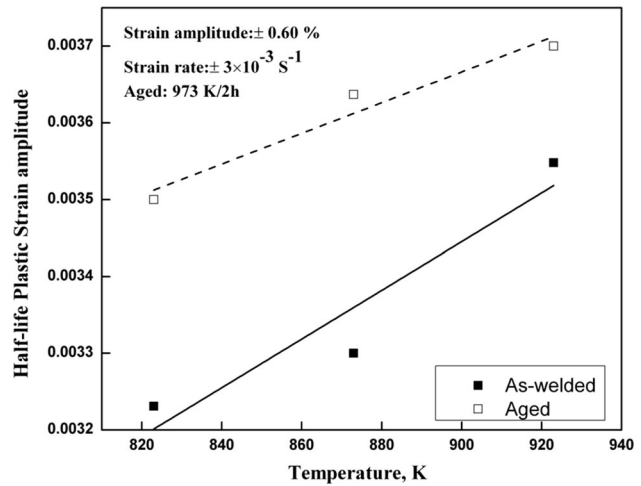


Fig. 18—Variation of half-life plastic strain amplitude with temperature ($\Delta\epsilon_i/2 = \pm 0.6$ pct).

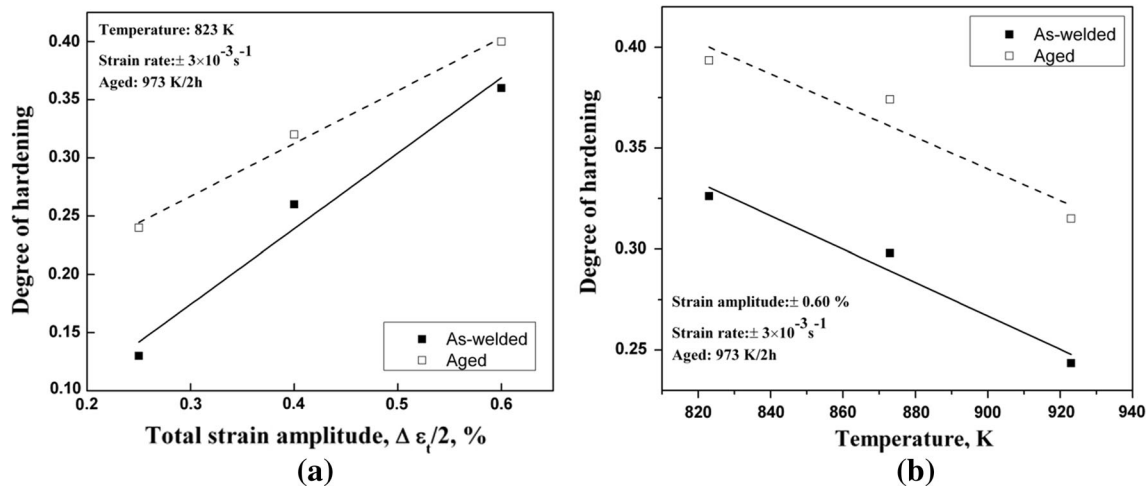


Fig. 17—(a) Degree of hardening vs strain amplitude for the as-welded and aged conditions, 823 K (550 °C) and (b) variation of the degree of hardening with temperature, ($\Delta\epsilon_i/2 = \pm 0.6$ pct).

Table IV. The δ -Ferrite Content (FN) and Percentage of Transformation after LCF Testing at Different Temperatures and Strain Amplitudes

Temperature, K (°C)	Strain Amplitude ($\pm \epsilon_t/2$), Pct	As-welded Condition		Aged Condition	
		FN	Percent Transformation of δ -Ferrite	FN	Percent Transformation of δ -Ferrite
823 (550)	0.25	5.3	26.4	2.7	3.6
	0.4	5.1	29.2	2.5	10.7
	0.6	4.3	40.2	1.8	35.7
873 (600)	0.25	4.8	33.3	2.5	10.7
	0.4	4.2	41.6	2.3	17.8
	0.6	3.9	45.8	1.4	50
923 (650)	0.25	3.4	52.8	2.1	25
	0.4	3.1	57	1.7	39.3
	0.6	2.1	70.8	0.7	75

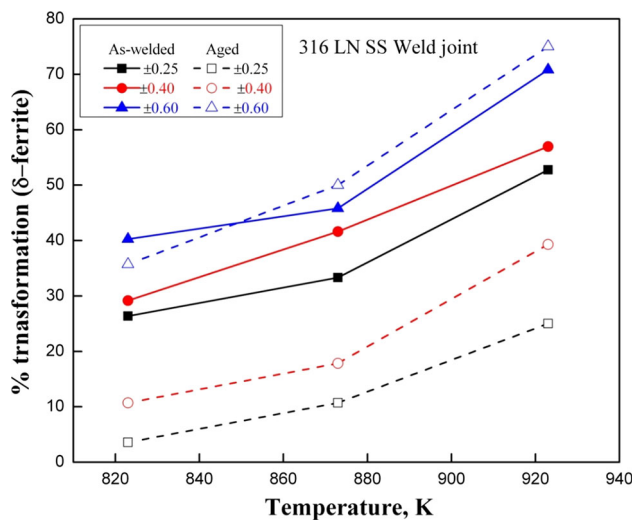


Fig. 19—Variation of δ -ferrite transformation during LCF loading under the as-welded and aged conditions.

operation leads to strain hardening effect in the initial weld passes resulting in complex dislocation patterns that led to higher initial hardness in the weld region as shown in Figure 5. The changes observed in dislocation structure during cyclic loading depend on the initial microstructure of the material.^[38] During cyclic loading, dislocation tangles break down and subsequent annihilation of dislocations of opposite sign occurs during their to-and-fro motion. This leads to a general reduction in the dislocation density after LCF, as reflected from the TEM micrographs presented in Figures 21 and 22(a) and (b). As seen from Figure 21, dislocations rearranged themselves into a crude cell formation leading to a drastic reduction in the dislocation density compared to that under the initial condition.

It may be recalled that the period of cyclic hardening was lower in the as-welded condition compared with the aged condition (Figure 14) which could be ascribed to the cast structure and a higher dislocation density in the

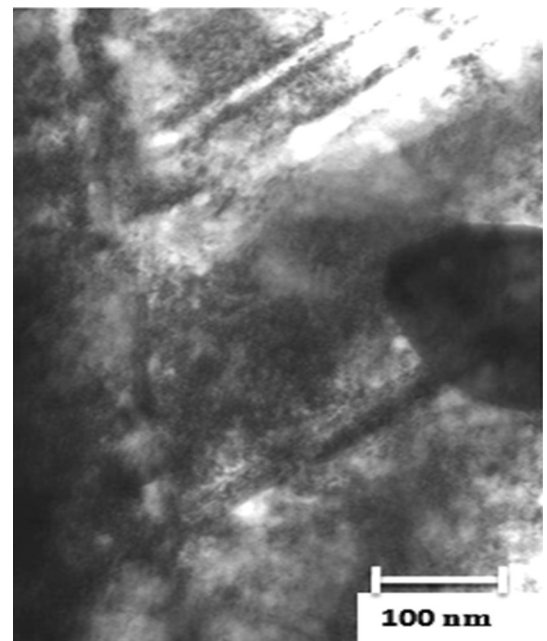


Fig. 20—TEM micrograph of the weld metal region (as-welded condition).

former. A comparison of the TEM images presented in Figures 21 and 22(a) and (b) underlines the difference in the dislocation substructure associated with cyclic deformation in the as-welded and aged conditions. The dislocation density was seen to be higher in the aged condition compared with the as-welded condition. Besides, the cell structure was seen to have developed more clearly in the aged condition (Figures 22(a) and (b)) compared with the as-welded (Figure 21) case. It may be noted that an increase in the dislocation density with cyclic deformation increases the driving force for dislocation rearrangement, leading to the formation of a cell structure.^[16] The development of a clear cell structure in the aged condition compared with the as-welded condition presumably resulted from the more extensive deformation in the weld zone in the former case. The extended period of cyclic hardening in the

aged condition is attributed to the initial lower dislocation density and a subsequent increase in the same, during cyclic loading.

The weld joint specimen in the as-welded condition showed a rapid cyclic softening. The extent of cyclic softening was lower in the aged condition, as shown in Figure 15(b). With an increase in test temperature, the plastic strain accumulation at half-life was observed to increase at a higher rate in the as-welded compared with the aged condition (Figure 18) which could be the result of a change in the initial structure of the weld region following the prior thermal exposure. Cyclic deformation of the aged weld joint at a strain amplitude of ± 0.6 pct led to a well-developed subcell structure, characterized by a high dislocation density cell walls and a lower dislocation density interiors, as shown in Figures 22(a) and (b).

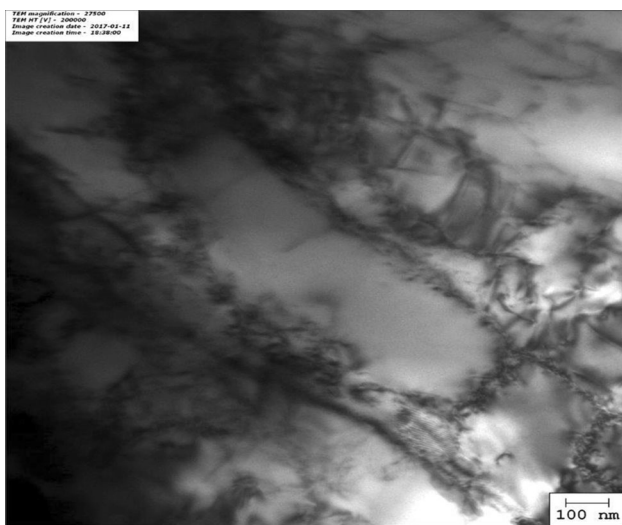


Fig. 21—TEM microstructure of the weld metal region showing dislocation annihilation/recovery after LCF cycling [923 K (650 °C), ± 0.6 pct, the as-welded condition].

H. Influence of Temperature

1. Strain-life variation

Downward shifts of the half-life stress and peak tensile stress were observed with the increasing test temperature as shown in Figures 16 and 23, respectively. Decreases in the peak and half-life tensile stresses and increase in the $\Delta\epsilon_p/2$, coupled with a decrease in the rate of cyclic hardening with the increasing temperature during LCF, emphasize the role of thermal recovery processes on cyclic deformation. These observations are in agreement with those reported by Reddy *et al.*^[39] and Shankar *et al.*^[40]

The cyclic life and location of failure were seen to depend on the relative damage accumulation in the constituents of the weld joint in response to the imposed strain cycles. The fatigue life varied inversely with the applied strain amplitude and temperature, as seen in Figure 24. It is well established that the cyclic life under LCF is a strong function of the tensile ductility of the material. In the present investigation, prior thermal aging at 973 K (700 °C) for 2 hours resulted in an increase in fatigue life compared with the as-welded condition. This behavior is similar to the findings of Liu *et al.*^[41] on 308 L weldments wherein it was observed that postweld heat treatment in the range 923 K to 1123 K (650 °C to 850 °C) for 1 hour, resulted in a lowering of the initial stress response accompanied by an increase in the creep-fatigue life. The increase in cyclic life observed in the present investigation after the prior thermal exposure could be attributed to a marginal increase in the ductility, together with a decrease in the YS of the weld joint. Besides, the reduction in the hardness of the weld region as a consequence of the thermal aging induced a higher plastic deformation in the aged weld joint in comparison with the as-welded material, as reflected from Figure 18. This effectively led to a considerable reduction in the severity of the metallurgical notch (as already explained in the Section III-E-2) and the associated strain incompatibility in the weld joint, thereby minimizing the stress concentration effects induced by the presence of different zones. The consequent uniformity of deformation across the

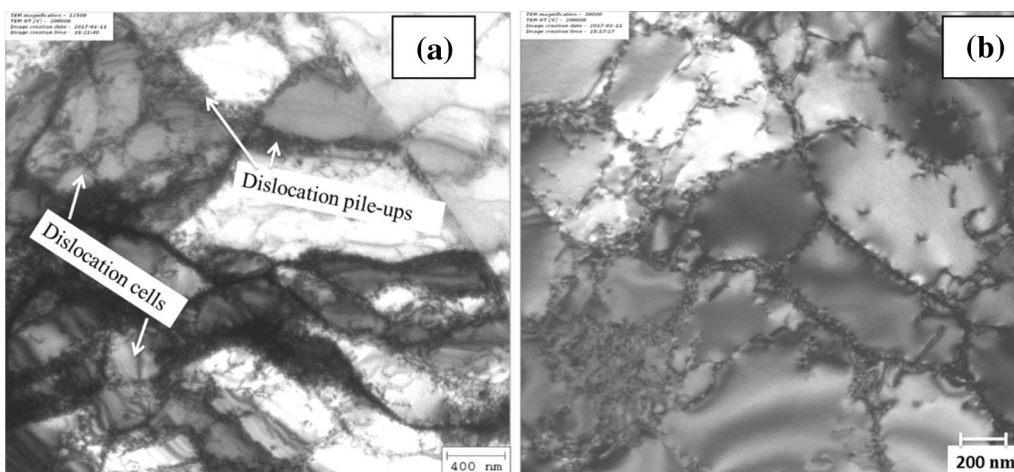


Fig. 22—(a, b) Well-developed dislocation cell structure obtained after LCF cycling [923 K (650 °C), ± 0.6 pct, aged condition].

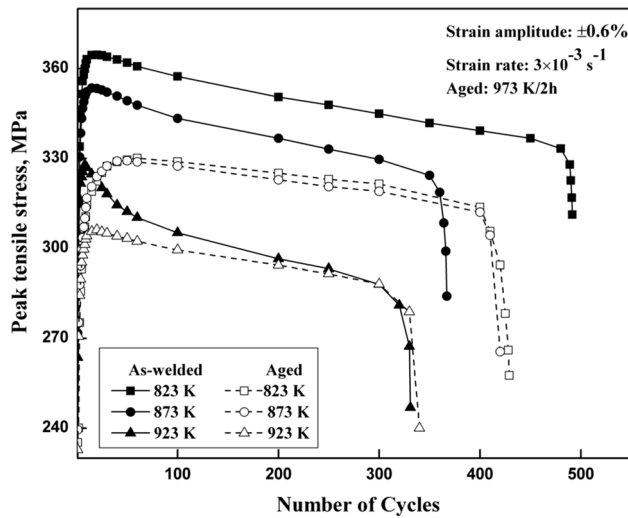


Fig. 23—Variation of cyclic stress response with temperature in the as-welded and aged conditions ($\Delta\epsilon_t/2 = \pm 0.6$ pct).

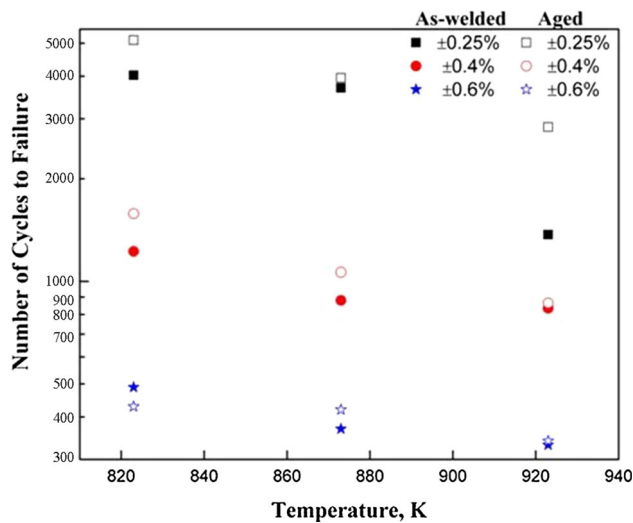


Fig. 24—Variation of fatigue life with temperature for different strain amplitudes in the as-welded and aged conditions.

thermally aged weld joint contributes to an enhancement in cyclic life under LCF, as evidenced from Figure 24. The reduction in fatigue life with increasing temperature can be attributed to a combined influence of increased plastic strain as a result of creep deformation and oxidation.^[32] The difference in LCF lives between the as-welded and aged conditions was observed to decrease with an increase in the applied strain amplitude, as seen from Figure 24. The larger difference observed at low-strain amplitudes is associated with the differential strain accumulation between the base and the weld portion of the weld joint. As observed in Section III-E-1, the base metal takes most of the imposed strain in the as-welded condition. Consequent to the thermal exposure, however, the weld metal starts participating in the cyclic deformation which effectively minimizes the strain localization effect, thereby leading to an enhancement in the cyclic life. The decrease in the difference in fatigue lives between the two conditions at higher strain amplitudes could be attributed to an increase in the secondary cracks in the as-welded condition (Figure 27(b)) and the embrittlement due to the formation of intermetallic phases and carbides, and the associated loss of ductility of the weld zone of the aged weld joint during the cyclic loading (as will be explained in the next section).

2. Crack initiation and propagation

Failure under cyclic loading is largely influenced by the initial microstructure of the material and its evolution as a function of both the time and the number of cycles. The crack initiation and propagation occurred in transgranular mode in all the three investigated temperatures. Figures 25(a) and (b) present the typical fracture surface morphology obtained at 823 K and 873 K (550 °C and 600 °C). It was observed that cycling at the lowest strain amplitude of ± 0.25 pct was characterized by stage-I crack propagation to a greater extent (Figure 25(a)), compared with higher strain amplitude (Figure 25(b)). In contrast, stage-II crack growth featuring well-developed striations dominated at the higher amplitudes of loading. Stage-II transgranular cracking

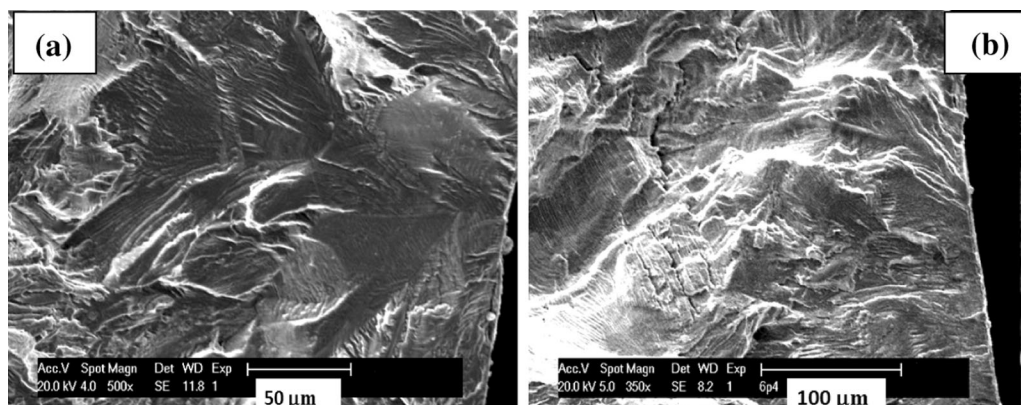


Fig. 25—(a) Crack initiation and stage-I propagation at 823 K (550 °C), ± 0.25 pct in the as-welded condition and (b) stage-I and stage-II cracking with multiple secondary cracks at 873 K (600 °C), ± 0.4 pct, aged condition.

was characterized by the occurrence of ductile striations on the fracture surface at the temperature— $\Delta\epsilon_i/2$ combination of 873 K (600 °C) and ± 0.6 pct in the as-welded condition as shown in Figure 26.

Failure occurred in the base metal region in both the as-welded and aged conditions at low-strain amplitudes. In the intermediate testing conditions, secondary cracks were observed in the base metal portion, in both the as-welded (Figures 27(a) and (b)) and aged (Figure 25(b)) specimens. It is to be noted that although the weld joint specimen is subjected to a constant cyclic strain, the response from the base metal and weld metal regions to the imposed strain is different as explained above. The distribution of strain in each zone depends on the relative stiffness of the weld metal with regard to the base metal. The resultant stress associated with low-strain LCF cycling is insufficient to cause significant deformation in the weld region due to the higher YS of

the weld metal compared with the base metal region, whereby most of the deformation gets concentrated in the base metal leading to failure in the latter as shown in Figures 27(a) and (b). However, as the strain amplitude increased, extensive cracking was observed along the σ/γ interface in the weld metal zone in the thermally aged condition as shown in Figures 28 (a) and (b).

It is also observed that the cracks generally followed the austenite and σ -phase interface in the weld metal. Number of crack initiation sites increased with an increase in temperature and strain amplitude in the aged condition. Figure 29 shows multiple crack initiation sites in the weld metal region of the sample tested at 923 K (650 °C), at $\Delta\epsilon_i/2 = \pm 0.6$ pct in the aged condition. The decomposition of δ -ferrite to σ -phase due to cycling loading leads to embrittlement at the interface between the remaining γ - and σ -phases. The significant strain incompatibility at the σ/γ interface resulted in stress concentration at the interface leading to crack initiation. It has been reported^[36] that the decomposition of δ -ferrite leads to a higher stress/strain concentration at the interfaces between δ -, σ -, and γ -phases in the weld zone. The microcracks, once initiated along the σ/γ interface, coalesce and grow rapidly, leading to failure along the interface. The weld zone showed substantial multiple cracking along the interstriation regions in the aged condition, as presented in Figure 30. The cyclic loading is known to accelerate the decomposition rate of δ -ferrite by two orders higher than thermal aging.^[36]

The investigation thus established the significant and decisive role played by the weld zone in dictating the global deformation response and thereby the resultant cyclic life, through aging-induced metallurgical changes occurring therein. Microstructural examination revealed that the σ -phase that formed from the parent δ -ferrite played a key role in the crack propagation during cyclic loading at the highest strain amplitude of ± 0.6 pct as shown in Figures 28(a) and (b), which clearly reveal the

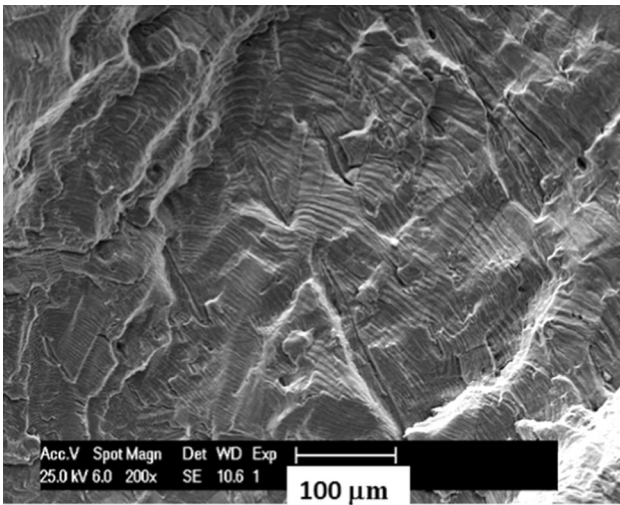


Fig. 26—Well-developed fatigue striations in base metal at 873 K (600 °C), ± 0.6 pct, as-welded condition.

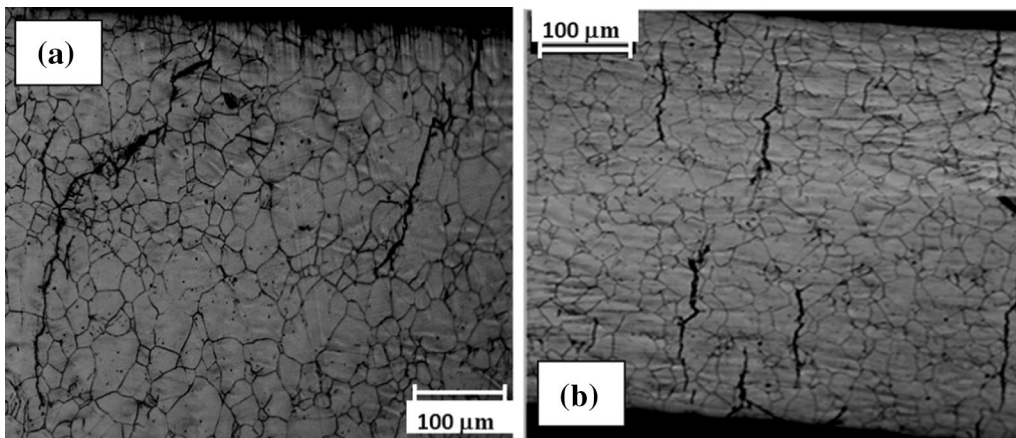


Fig. 27—Transgranular crack propagation in base metal (as-welded joint), (a) 823 K (550 °C), ± 0.25 pct and (b) 873 K (600 °C), ± 0.4 pct.

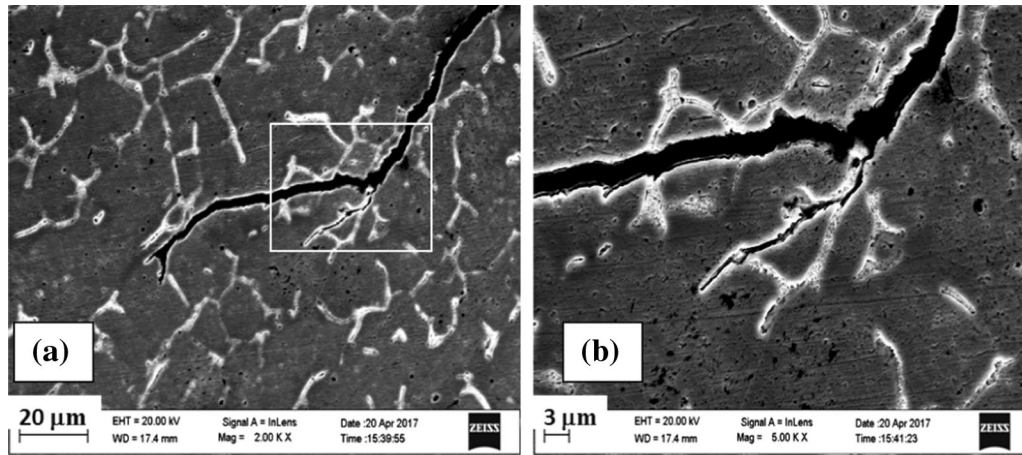


Fig. 28—(a) Cracks observed in the weld region at the strain amplitudes of ± 0.6 pct, 873 K (600 °C) in the thermally aged weld joint and (b) magnified view of the marked portion in (a) showing crack deflection in the weld region.

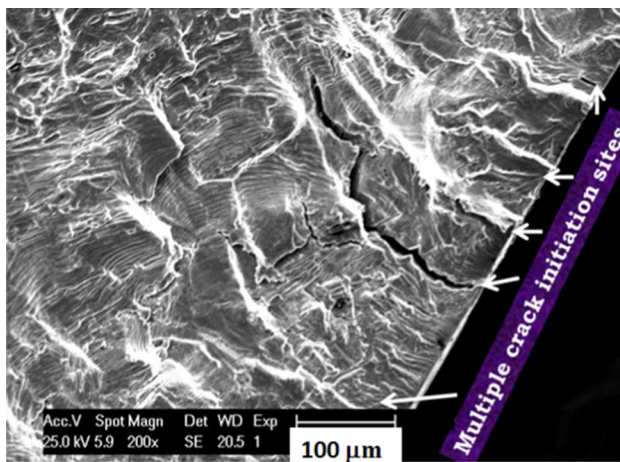


Fig. 29—Multiple crack initiation in the weld metal region (923 K (650 °C), ± 0.6 pct, aged condition).

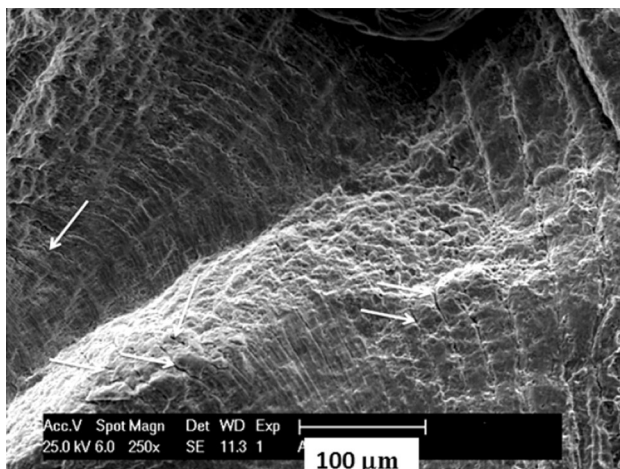


Fig. 30—Secondary cracks in the interstriation regions within the weld zone (indicated by arrows) at 923 K (650 °C), ± 0.60 pct, aged condition.

crack path along the stringers of σ -phase. The difference in the mechanical response between the hard σ and the softer γ -phase gets more pronounced during cyclic loading at the strain amplitude of ± 0.6 pct, as compared with the lower strain amplitudes, leading to crack formation within the weld zone and the eventual reduction in the difference in life between the as-welded and aged conditions. The σ -phase being hard and brittle, provides easy path for crack propagation. Besides, significant deflection of the crack path occurred due to the presence of σ -phase as shown in Figures 28(a) and (b). It was observed that the striation spacing increases with increase in the crack length (Figure 30) owing to the buildup of higher stress at the crack tip as it advances during successive cycles.

IV. CONCLUSIONS

1. Prior thermal exposure at 973 K (700 °C) for 2 hours resulted in a higher fatigue life of 316LN SS weld joint, compared with the as-welded condition.
2. Thermal aging imparted a softening effect on the weld metal, leading to an increase in the ductility of the weld joint. The increased ductility resulted in a slight lowering of the stress response in the aged condition.
3. The degree of cyclic hardening was seen to be marginally higher in the aged condition compared with the as-welded condition. Temperature, together with cyclic deformation, plays an important role on the extent of δ -ferrite transformation within the weld region.
4. Crack initiation occurred in the base metal region under all the testing conditions in the as-welded joint. However, the failure location shifted from the base metal to the weld region with an increase in the applied strain amplitude in the case of thermally aged weld joint.

5. Fatigue life decreased with the increasing temperature and strain amplitude in both the as-welded and aged conditions. Reduction in life at high strain amplitude in the thermally aged condition is associated with failure in the weld metal region.
6. Automated ball-indentation technique could be used as a tool to understand the strain partitioning between different zones of the weld joint. The base metal takes most of the applied cyclic strain during LCF deformation in the as-welded condition. However, embrittlement occurred in the weld metal during cyclic loading in the aged condition.

ACKNOWLEDGMENTS

The authors wish to acknowledge the valuable suggestions from Dr. G. Sasikala and Dr. B.K. Panigrahi. Helpful discussion with Mr. R. Kannan and the experimental supports received from Mr. V. Ganesan and Mr. M. Srinivasa Rao are also gratefully acknowledged. Valuable support from the Central Workshop Division, IGCAR in the fabrication of the weld pads is also acknowledged. One of the authors (TSK) acknowledges the research fellowship granted by the Homi Bhabha National Institute.

ANNEXURE-I

The measured value of total indentation depth (h_t) was converted into total indentation diameter (d_t) using Eq. [1] as follows^[42]:

$$d_t = 2(Dh_t - h_t^2) \quad [1]$$

where D is the diameter of the indenter.

Yield Strength

In the ABI test, both elastic and plastic deformations occur simultaneously in each cycle, with simultaneous yielding and work hardening taking place in each cycle.^[19] During the calculation of yield stress, the occurrence of yielding in each cycle is taken into account by considering the entire load—displacement curve. The data points from the loading cycles were fit by linear regression to the following (Meyer) relationship between the mean pressure (P) and d_t ^[42]:

$$\frac{P}{d_t^2} = A \left(\frac{d_t}{D} \right)^{m-2}, \quad [2]$$

where m is the Meyer's exponent (m generally varies between 2 and 2.5) and A is a material yield parameter obtained from the regression analysis. The yield strength (σ_y) is proportional to the Meyer hardness ($4P/pd_t^2$), and can be written as^[42]

$$\sigma_y = \beta_n \cdot A, \quad [3]$$

where β_n is a constant for a given class of materials. The value of β_n for each class of materials is determined from the YS obtained from the standard tensile tests, and the value of A is obtained from the ABI tests.

Ultimate Tensile Strength

Under compressive loading, since the material does not undergo necking, the UTS is determined in an indirect way. The strain hardening exponent (n) is equal to the true uniform strain (ϵ_u) at the UTS of the material under tensile loading. The engineering UTS (S_{UTS}) can be obtained by equating $\epsilon_u = n$ in the Hollomon equation^[43] as follows:

$$S_{UTS} = K \left(\frac{n}{e} \right)^n. \quad [4]$$

The UTS can be derived from the above equation only for a material the stress–strain curve of which obeys the Hollomon equation.

True Plastic Strain

The value of plastic indentation diameter (d_p) was calculated from the plastic indentation depth (h_p) by iterating the following equation^[19]:

$$d_p = \sqrt[3]{(2.735 P D) \frac{[1/E_{\text{spec}} + 1/E_{\text{ind}}] [4h_p^2 + d_p^2]}{4h_p^2 + d_p^2 - 4h_p D}}, \quad [5]$$

where P is the applied load, E_{spec} and E_{ind} are the Young's Moduli of the specimen and the indenter, respectively. Loading followed by partial unloading during indentation enables the determination of h_p .

Tabor^[44] established the following correlation between true plastic strain ϵ_p in a uniaxial tensile test and indentation strain (d_p/D) from a ball-indentation test:

$$\epsilon_p = 0.2(d_p/D) \quad [6]$$

True Stress

Using the maximum shear stress theory as the yielding criterion, the true stress σ_t is given by

$$\sigma_t = \frac{4P}{\pi d_p^2 \delta}, \quad [7]$$

where δ is a constant related to the constraint effect for plastic deformation for a given class of material. The δ parameter correlates the hardness or mean pressure to the true flow stress and depends on the strain rate sensitivity and work hardening characteristics of the

material being tested. Typically, it varies from 0.90 to 1.25 for structural steels.^[18] In the current study, the value of δ was found to be 0.95.

REFERENCES

1. S.L. Mannan, S.C. Chetal, B. Raj, and S.B. Bhoje: *Trans. Indian Inst. Met.*, 2003, vol. 56, pp. 155–78.
2. E. Folkhard: *Welding Metallurgy of Stainless Steels*, Springer Verlag Wein, New York, NY, 1988.
3. R.G. Thomas and D. Yapp: *Weld. J.*, 1978, vol. 57, pp. 361–66.
4. V.S. Raghunathan, V. Seetharaman, S. Venkadesan, and P. Rodriguez: *Metall. Trans. A*, 1979, vol. 10A, pp. 1683–89.
5. G.F. Slattery, S.R. Keown, and M.E. Lambert: *Met. Technol.*, 1983, vol. 10, pp. 373–85.
6. T.P.S. Gill, M. Vijayalakshmi, J.B. Gnanamoorthy, and K.A. Padmanabhan: *Weld. Res. Suppl.*, 1986, vol. 65, pp. 122–28.
7. M.O. Malone: *Weld. J. Res. Suppl.*, 1967, vol. 46, pp. 241–53.
8. H. Shaikh, M.G. Pujar, N. Sivaibarasi, P.V. Sivaprasad, and H.S. Khatak: *Mater. Sci. Tech.*, 1994, vol. 10, pp. 1096–1103.
9. J.J. Smith and R.A. Farrar: *Int. Mater. Rev.*, 1993, vol. 38 (1), pp. 25–51.
10. S. Kožuh, M. Gojić, and L. Kosec: *Kovove Mater.*, 2009, vol. 47, pp. 253–62.
11. M. Valsan, D. Sundararaman, K. Bhanu Sankara Rao, and S.L. Mannan: *Metall. Mater. Trans. A*, 1995, vol. 26A, pp. 1207–19.
12. E. Yoshihisa and S. Ganesh Sundara Raman: *Sci. Technol. Weld. Join.*, 2000, vol. 5, pp. 174–82.
13. G.V. Prasad Reddy, R. Sandhya, M. Valsan, and K.B.S. Rao: *Int. J. Fatigue*, 2008, vol. 30, pp. 538–46.
14. S.K. Chandra, V. Shankar, K. Mariappan, R. Sandhya, and P.C. Chakraborty: *Proc. Eng.*, 2013, vol. 55, pp. 176–80.
15. K. Bhanu Sankara Rao, M. Valsan, and S.L. Mannan: *Mater. Sci. Eng. A*, 1990, vol. 130, pp. 67–82.
16. H. Wang, H. Jing, L. Zhao, Y. Han, X. Lv, and L. Xu: *Mater. Sci. Eng. A*, 2017, vol. 690, pp. 16–31.
17. M.D. Mathew, G. Sasikala, S.L. Mannan, and P. Rodriguez: *Mater. Sci. Technol.*, 1991, vol. 7 (6), pp. 533–36.
18. S. Goyal, R. Sandhya, M. Valsan, and K. Bhanu Sankara Rao: *Int. J. Fatigue*, 2009, vol. 31, pp. 447–54.
19. F.M. Haggag, R.K. Nanstad, J.T. Hutton, D.L. Thomas, and R.L. Swain: in *Applications of Automation Technology to Fatigue and Fracture Testing*, ASTM 1092, A.A. Braun, N.E. Ashbaugh, and F.M. Smith, eds., American Society for Testing and Materials, Philadelphia, 1990, pp. 188–208.
20. F.M. Haggag: in *Small Specimen Test Techniques Applied to Nuclear Reactor Vessel Thermal Annealing and Plant Life Extension*, ASTM STP 1204, W.R. Corwin, F.M. Haggag, and W.L. Server, eds., American Society for Testing and Materials, Philadelphia, 1993, pp. 27–44.
21. M.D. Mathew, K.L. Murthy, L.M. Lietzan, and V.N. Shah: *Mater. Sci. Eng. A*, 1999, vol. 269, pp. 186–96.
22. M.D. Mathew, K.L. Murthy, K.B.S. Rao, and S.L. Mannan: *Mater. Sci. Eng. A*, 1999, vol. 264, pp. 159–66.
23. K.L. Murthy, P.Q. Miraglia, M.D. Mathew, V.N. Shah, and F.M. Haggag: *Int. J. Press. Vess. Pip.*, 1999, vol. 76, pp. 361–69.
24. G. Das, M. Das, S. Sinha, K.K. Gupta, S. Chakraborty, and A.K. Ray: *Mater. Sci. Eng. A*, 2009, vol. 51, pp. 389–93.
25. J.F. Zarzour, P.J. Konkol, and H. Dong: *Mater. Charact.*, 1996, vol. 37, pp. 195–209.
26. J. Ganesh Kumar, V.D. Vijayanand, M. Nandagopal, and K. Laha: *Mater. High Temp.*, 2015, vol. 32, pp. 619–26.
27. H.K. Khandelwal, K. Sharma, and R. Chhibber: *J. Miner. Mater. Charact. Eng.*, 2012, vol. 11, pp. 1095–1100.
28. S. Wu, T. Xu, M. Song, and K. Guan: *Mater. High Temp.*, 2016, vol. 33, pp. 270–75.
29. T.P.S. Gill, M. Vijayalakshmi, P. Rodriguez, and K.A. Padmanabhan: *Metall. Mater. Trans. A*, 1989, vol. 20A, pp. 1115–24.
30. V.S. Srinivasan, M. Valsan, R. Sandhya, K. Bhanu Sankara Rao, S.L. Mannan, and D.H. Sastry: *Int. J. Fatigue*, 1999, vol. 21, pp. 11–21.
31. G.V. Prasad Reddy, R. Sandhya, S. Sankaran, and M.D. Mathew: *Metall. Mater. Trans. A*, 2014, vol. 45A, pp. 5044–56.
32. V.S. Srinivasan, R. Sandhya, K. Bhanu Sankara Rao, S.L. Mannan, and K.S. Raghavan: *Int. J. Fatigue*, 1991, vol. 13, pp. 471–78.
33. D. Sundararaman, P. Shankar, and V.S. Raghunathan: *Metall. Mater. Trans. A*, 1996, vol. 27A (5), pp. 1175–86.
34. D.W. Kim, W.-S. Ryu, J.H. Hong, and S.K. Choi: *J. Nucl. Mater.*, 1998, vol. 254, pp. 226–33.
35. V.S. Srinivasan, R. Sandhya, M. Valsan, K.B.S. Rao, S.L. Mannan, and D.H. Sastry: *Scripta Mater.*, 1997, vol. 37 (10), pp. 1593–98.
36. S. Hasebe and T. Asayama: *Mater. Sci. Res. Int.*, 1997, vol. 3 (3), pp. 178–84.
37. G. Sasikala, S.K. Ray, and S.L. Mannan: *Mater. Sci. Eng. A*, 2003, vol. 359, pp. 86–90.
38. C. Laird, Z. Wang, B.T. Ma, and H.F. Chai: *Mater. Sci. Eng. A*, 1989, vol. 113, pp. 245–57.
39. G.V. Prasad Reddy, R. Sandhya, M. Valsan, and K.B.S. Rao: *Mater. Sci. Technol.*, 2010, vol. 26, pp. 1384–92.
40. V. Shankar, K. Mariappan, R. Sandhya, and K. Laha: *Int. J. Fatigue*, 2016, vol. 82, pp. 487–96.
41. F. Liu, Y.H. Hwang, and S.W. Nam: *Mater. Sci. Eng. A*, 2006, vol. 427, pp. 35–41.
42. E. Meyer and D. Zeits: *Ver. Deut. Ing.*, 1980, vol. 52, p. 645.
43. ASTM E646-07: 'Standard test method for tensile strain hardening exponents (n -values) of metallic sheet materials'; 2007, Philadelphia, American Society for Testing and Materials.
44. D. Tabor: *The Hardness of Metals*, Oxford University Press, New York, NY, 1951.